ACS APPLIED MATERIALS & INTERFACES

Research Article

www.acsami.org

Attomolar Level Detection of Raman Molecules with Hierarchical Silver Nanostructures Including Tiny Nanoparticles between Nanosized Gaps Generated in Silver Petals

Anirban Dandapat,[†] Tae Kyung Lee,[‡] Yiming Zhang,[†] Sang Kyu Kwak,*[,‡] Eun Chul Cho,*[,§] and Dong-Hwan Kim*[,†]

[†]School of Chemical and Biomedical Engineering, Nanyang Technological University, Singapore 637457, Singapore

[‡]School of Energy and Chemical Engineering, Ulsan National Institute of Science and Technology (UNIST), 50 UNIST-gil, Ulsan 689-798, South Korea

[§]Department of Chemical Engineering, Hanyang University, Seoul 133-791, South Korea

Supporting Information

ABSTRACT: We developed a route for synthesizing Ag nanostructures with tunable morphologies for ultrasensitive surface-enhanced Raman spectroscopy. Through the consecutive addition of three reducing agents (i.e., 4-mercaptobenzoic acid, trisodium citrate, and ascorbic acid) to an aqueous solution of silver nitrate, hierarchical flower-like Ag nanostructures were produced. The nanostructures had Ag petals in which nanosized gaps were generated, and small Ag nanoparticles were incorporated within the gaps. Theoretically, the nanostructures exhibited highly enhanced electric fields in the outer-shell regions where the small Ag nanoparticles were densely located. Combining the enhanced field effect with resonance effect of a Raman-active molecule (methylene blue) at a specific wavelength, measurable Raman signals were obtained at concentrations as low as 100 attomolar (10^{-16} M; corresponding to 10^{-21} mol). Key factors were discussed for the synthesis of the Ag nanostructures while finely controlling the morphologies of hierarchical Ag nanostructures, thereby modulating the intensity of surface-enhanced resonance Raman spectroscopy (SERRS) signals. Therefore, this synthetic method produces highly promising nanostructures for SERRS-based applications.

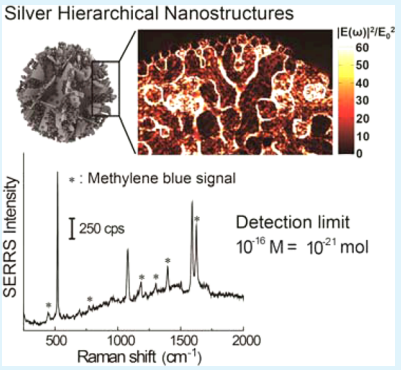

KEYWORDS: *silver nanostructures, morphology tuning, nanoparticles incorporated branches, ultrasensitive detection, SERRS*

1. INTRODUCTION

The detection of Raman-active molecules with high sensitivity has become an important issue in various biosystems and other areas.[1−6] The detection sensitivity of trace Raman molecules can be enhanced by either modifying the geometries of plasmonic nanoparticles (Ag- and Au-based)[6−8] or constructing structures from these nanoparticles.[9−16] The improvements rely mostly on the enhancement of the electric field developed on nanoparticles or nanostructures.[17−19] Most efforts have been devoted to modulating gap distances between nanoparticles to enhance the electric field.[9−16] Recently, it was reported that a superhydrophobic plasmonic patterned structure could also help increase detection sensitivity of Raman molecules,[20] and generation of nanosized gaps within plasmonic nanoparticles could both increase the sensitivity of substrates for Raman-active molecules and enhance the reproducibility of SERS-active sites.[21] These understandings of signal enhancement allow for the detection of Raman molecules at the zeptomole level[16] or even lower.[20]

In this study, we present that the inclusion of Ag nanoparticles between nanosized gaps generated in Ag nanostructures (Scheme 1) could also greatly enhance electric fields of the Ag nanostructures and thus they could serve as substrates for ultrasensitive surface-enhanced resonance Raman spectroscopy (SERRS).[22−25] The Ag nanostructures are synthesized on a wet basis and are composed of Ag petals in which nanosized gaps (∼20 nm in average) are generated, and small Ag nanoparticles (5−10 nm) are included between the gaps. Theoretical studies confirmed that the nanostructures exhibit highly enhanced electric fields, especially in the outer-shell regions where small Ag nanoparticles are densely located. With a laser wavelength at which a Raman-active dye can highly absorb, significant SERRS enhancement was obtained not only due to the hot spots generated by the small Ag nanoparticles in the Ag petals but also due to the resonance effect of the dye. Therefore, measurable Raman signals from methylene blue with concentrations as low as 100 attomolar (10^{-16} M; corresponding to 10^{-21} mol) were obtained. This result can be considered the state-of-the-art level of sensitivity, and only a few studies have reported such comparable achievements.[16,20] In addition,

Received: April 10, 2015
Accepted: June 24, 2015
Published: June 24, 2015

DOI: 10.1021/acsami.5b03109
ACS Appl. Mater. Interfaces 2015, 7, 14793−14800

Scheme 1. Schematic Representation Showing a Route for Synthesizing Hierarchical Ag Nanostructures and the Simulated Electric Field Distribution in the Corresponding Region

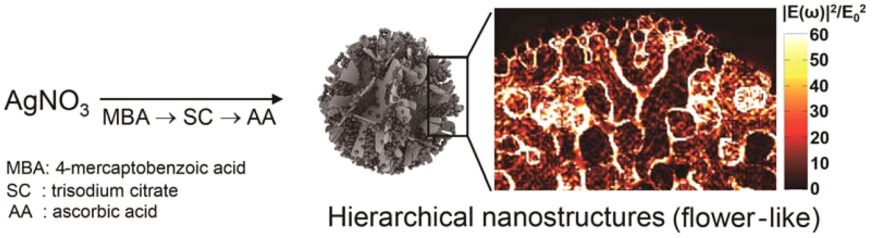

herein, key factors were discussed while finely controlling the morphologies of hierarchical Ag nanostructures, thereby modulating the intensity of SERRS signals.

2. EXPERIMENTAL SECTION

Materials. $AgNO_3$ (≥99%, Sigma-Aldrich) (90%, Aldrich), sodium citrate tribasic dihydrate (≥98%, Sigma-Aldrich), L-ascorbic acid (99%, Acros Organic), hydrogen peroxide (H_2O_2, 30 wt % in water Merck), sulfuric acid (H_2SO_4, 95−98%, Sigma-Aldrich), aminopropyltriethoxysilane (APTES, ≥98%, Sigma-Aldrich), and methylene blue (≥95%, Fluka) were used as received.

Synthesis of Nanostructures. In a typical experiment, an ethanolic solution of MBA was mixed with an aqueous solution of $AgNO_3$ (10 mM). After 5 min, different amounts of SC (30 mM) were added and stirred for another 5 min. Finally, freshly prepared L-ascorbic acid (10 mM) was added under stirring at room temperature, and it was continually stirred for 1 min and then placed undisturbed for 1 h. The resulting particles were centrifuged and redispersed repeatedly in deionized water and ethanol alternatively to remove excess surfactant. Before characterization, the samples were dried in a vacuum environment to prevent the oxidation on the Ag surface.

Characterization. Field-emission scanning electron microscopy (FE-SEM) was performed on the JEOL instrument (JSM-6700F) at an acceleration voltage of 5 kV and a working distance between 7 and 8 mm. The powder X-ray diffraction pattern was recorded on a Philips PW 1140 X-ray diffractometer using Cu Kα radiation (λ = 1.5406 Å). Transmission electron microscopic (TEM) studies were carried out by using a JEOL JEM-2100 microscope working at 100 kV. Raman spectra were collected using a Renishaw inVia confocal Raman spectrometer mounted on a Leica microscope with a 50× objective lens (NA = 0.80) in the range of 100−2000 cm^{-1} with one accumulation and a 10 s exposure time. A 633 nm wavelength HeNe laser (85 μW at the sample surface) was used to excite the sample.

Substrate Preparation for SERRS Studies. Ag nanostructures were coated on a silicon substrate (5 mm × 5 mm) for SERRS studies. First, the substrates were cleaned in a "piranha" bath (30% H_2O_2 and concentrated H_2SO_4 was mixed in the ratio of 1:4) at 60 °C for 15 min and then thoroughly rinsed with water and ethanol. (CAUTION: "Piranha" solution reacts violently with organic materials; it must be handled with extreme care.) To achieve the uniform coating of Ag nanostructures on the silicon substrate, the substrate was modified with APTES by dipping it in 10% APTES solution in ethanol for 1 h, washing with ethanol under sonication, drying at 120 °C for 30 min, and cooling to room temperature. Then, the surface-modified silicon substrate was dipped in a Ag nanostructure aqueous dispersion for 30 min, washed with water, and dried under vacuum. Then, 10 μL of aqueous methylene blue solution was deposited and dried under vacuum.

Discrete Dipole Approximation (DDA). It divides an arbitrary shape of target structure into finite cubic arrays of dipoles, which respond to the external electric field by forming dipole moments.[26−29] In DDA, optical spectra (i.e., extinction, absorption, scattering) and local electric field of target structure are calculated by the following step. The dipole moment P_{ia} induced by local electric field is expressed as

$$P_i = \alpha_i E_{loc}(r_i) \tag{1}$$

where α_i is the polarizability tensor and $E_{loc}(r_i)$ is the external electric field at the position of dipole r_i with i = 1, 2, 3···N. Clausius-Mossotti polarizability[29,30] is used for α_i, which is expressed as

$$\alpha_i = \frac{3d^3}{4\pi}\frac{\varepsilon_i - 1}{\varepsilon_i + 2} \tag{2}$$

where ε_i is the dielectric function of target structure. $E_{loc}(r_i)$ is the sum of the incident electric field ($E_{inc,i}$) and the dipole field; thus, P_i becomes

$$P_i = \alpha_i\left(E_{inc,i} - \sum_{\substack{j=1 \\ i\neq j}}^{N} A_{ij}P_j\right) \tag{3}$$

Eq 3 can be rearranged to be

$$\sum_{j=1}^{N} A_{ij}P_j = E_{inc,i} \tag{4}$$

Eq 4 is solved by the iteration scheme in the DDA method; then, the extinction cross-section is obtained by the following expression

$$C_{ext} = \frac{4\pi k}{|E_{inc}|^2}\sum_{j=1}^{N}\mathrm{Im}(E^*_{inc,j}P_j) \tag{5}$$

In this paper, we use the Discrete Dipole Scattering (DDSCAT) program, which performs DDA, developed by Drain and Flatau.[31,32]

Computation Details. We use the dielectric function (ε) of Ag from Johnson and Christy's work.[33] The ambient medium is air, of which the refractive index is taken to be 1.00028. The SERS enhancement factor of particular nanostructure can be approximated by the following expression,[34]

$$\phi = (|E(\omega)|^2/{E_0}^2) \times (|E(\omega')|^2/{E_0}^2) \tag{6}$$

where $|E(\omega)|^2/{E_0}^2$ is the local enhancement factor, $|E(\omega')|^2/{E_0}^2$ is the Stokes-shifted enhancement factor, E_0 represents a reference, which is the incident electric field, and the incident and Stokes-shifted frequencies are ω and ω', respectively. Stokes-shift frequency is 1624 cm^{-1} in this paper.

3. RESULTS AND DISCUSSION

For the synthesis of the Ag nanostructures, we successively added three types of reducing agents, i.e., 4-mercaptobenzoic acid (MBA), trisodium citrate, and ascorbic acid, to an aqueous solution of silver nitrate ($AgNO_3$) at room temperature. Figure 1a shows photographs showing the color changes of the aqueous solution at every addition step of each reducing agent. When 1 mL of 1 mM MBA ethanolic solution was added to 1 mL of 10 mM $AgNO_3$, small nanoparticles (8.8 ± 6.4 nm) were produced (Figure 1b). The nanoparticles showed a clear twinned boundary, implying that they were formed from more than two Ag seeds. The surfaces of the Ag nanoparticles were

DOI: 10.1021/acsami.5b03109
ACS Appl. Mater. Interfaces 2015, 7, 14793−14800

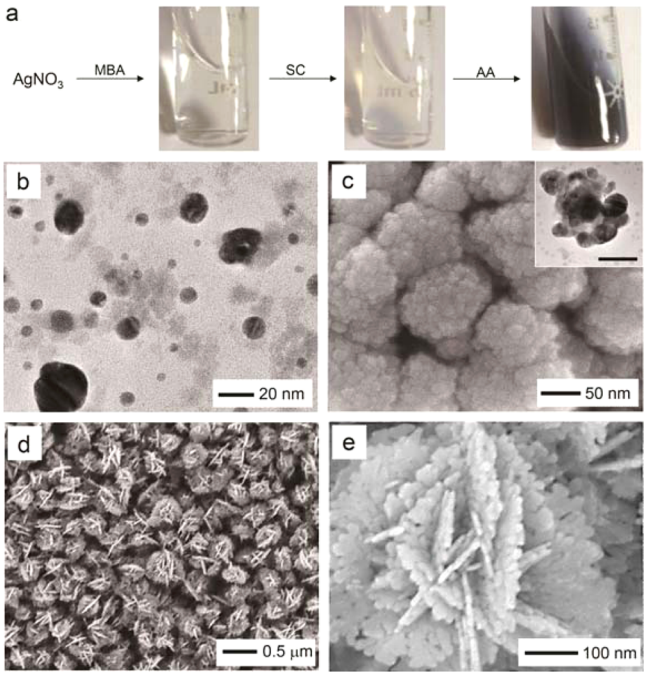

Figure 1. (a) Photographs showing the color changes of the reaction medium and (b–d) TEM and SEM images showing the morphology changes of Ag nanostructures during the consecutive addition of (b) 1 mL of 1 mM MBA solution, (c) 200 μL of 30 mM trisodium citrate (SC), and (d) 1 mL of 10 mM ascorbic acid (AA) to 1 mL of 10 mM $AgNO_3$. (e) Shows a magnification of the SEM image shown in (d). The scale bar in the inset of (c) is 50 nm.

expected to have been modified with a mixture of acid and thiol groups either via an Ag–thiol chemical bond or by the adsorption of carboxylic acid on the nanoparticle surfaces. The solution mixture appeared transparent. Because significantly larger mole numbers of Ag^+ than MBA were used in the system (i.e., 10 and 1 μmol, respectively), a considerable amount of Ag^+ still remained in the aqueous mixture.

By the subsequent addition of 200 μL of 30 mM trisodium citrate to the aqueous mixture, a portion of the remaining Ag^+ ions was reduced to form raspberry-like nanoparticle clusters (79 ± 20 nm, Figure 1c). As shown in the TEM image (inset), a number of large (~30 nm) and small (~15 nm) Ag nanoparticles randomly aggregated to form clusters, and the solution mixture subsequently became milky. The subsequent addition of 1 mL of 10 mM ascorbic acid to the aqueous dispersion changed the color of the solution to a bluish hue. The nanoclusters were transformed into hierarchical nanostructures measuring 400 ± 55 nm (Figure 1d; referred to as Ag-$M_1C_6A_{10}$, implying that 1, 6, and 10 μmol of MBA, trisodium citrate, and ascorbic acid were, respectively, used). As shown in the magnified SEM image (Figure 1e), the nanostructures appeared flower-like and each petal was highly branched, creating many gaps in the petal. The X-ray diffraction pattern (Figure S1, Supporting Information) of the nanostructures showed sharp peaks at 2θ values of 38.1°, 44.3°, 64.5°, 77.4°, and 81.5°, which are well indexed to the (111), (200), (220), (311), and (222) planes, respectively, for face-centered cubic Ag crystals; thus, it was confirmed that the developed nanostructures were crystalline in nature.[35,36]

On the basis of a number of experiments in which the ratio of the three reducing agents was varied, we found that the size and morphology of the Ag nanoclusters produced from the consecutive addition of MBA and trisodium citrate could affect the final morphologies of the hierarchical Ag nanostructures. In particular, the morphologies of the Ag nanostructures could be finely regulated by the molar ratios of trisodium citrate to MBA. Figure 2a plots the average sizes of the nanoclusters as a

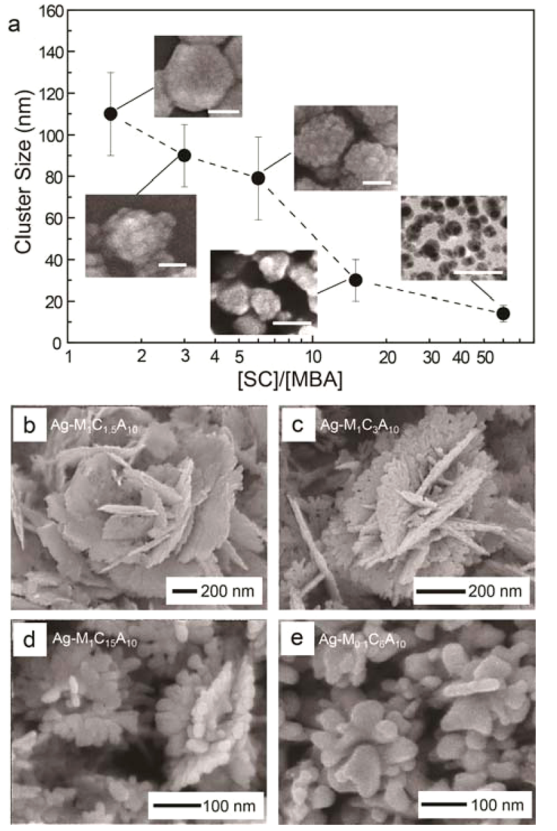

Figure 2. (a) Plot showing the sizes of Ag nanoclusters synthesized after the consecutive addition of MBA and trisodium citrate for various molar ratios of trisodium citrate (SC) to MBA. Insets show SEM and TEM images of nanoclusters for each composition (scale bar: 50 nm). (b–d) SEM images of Ag nanostructures containing different amounts of trisodium citrate (30 mM): (b) 50 μL, (c) 100 μL, and (d) 500 μL. The amounts of MBA (1 mL of 1 mM) and ascorbic acid (1 mL of 10 mM) were held constant. (e) SEM image of an Ag nanostructure produced with 1 mL of 0.1 mM MBA, 200 μL of 30 mM trisodium citrate, and 1 mL of 10 mM ascorbic acid.

function of the trisodium citrate to MBA molar ratios. The insets show SEM and TEM images that illustrate the corresponding morphologies of the nanoclusters. Overall, a larger molar ratio of trisodium citrate to MBA led to the formation of smaller Ag nanoclusters. When 1 μmol of MBA and 1.5 μmol of trisodium citrate were used (ratio: 1.5), large Ag clusters (110 ± 20 nm) containing small Ag nanoparticles (5–10 nm) on the surface were formed. The resulting Ag nanostructures appeared flower-like (1.3 ± 0.2 μm) with large and smooth petals (Figure 2b; referred to as Ag-$M_1C_{1.5}A_{10}$). When the amount of trisodium citrate was increased to 3 μmol (ratio: 3), 15–20 nm particles were assembled into raspberry-like clusters (90 ± 15 nm) and the corresponding Ag nanostructures (Figure 2c; referred to as Ag-$M_1C_3A_{10}$) were branched, similarly to those shown in Figure 1d (Ag-$M_1C_6A_{10}$) but larger (0.58 ± 0.1 μm). The clusters and resulting Ag nanostructure obtained at a ratio of 6 are shown in Figure 1. With 15 μmol of trisodium citrate (ratio: 15), the cluster size

DOI: 10.1021/acsami.5b03109
ACS Appl. Mater. Interfaces 2015, 7, 14793–14800

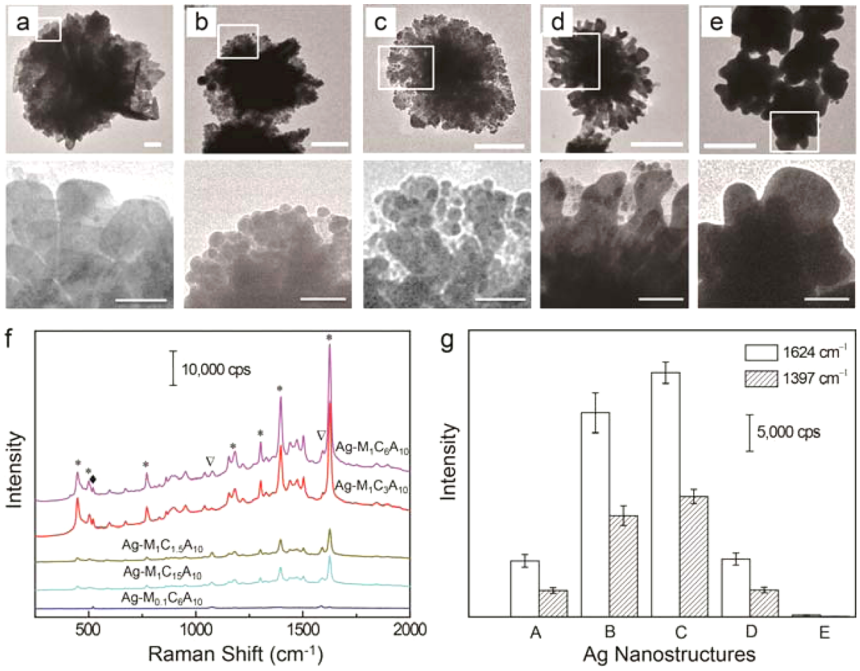

Figure 3. TEM images of hierarchical Ag nanostructures: (a) Ag-$M_1C_{1.5}A_{10}$, (b) Ag-$M_1C_3A_{10}$, (c) Ag-$M_1C_6A_{10}$, (d) Ag-$M_1C_{15}A_{10}$, and (e) Ag-$M_{0.1}C_6A_{10}$. Scale bars are (top) 200 nm and (bottom) 50 nm. (f) SERRS spectra of the five Ag nanostructures treated with 10^{-8} M methylene blue. Raman peaks of methylene blue (∗), MBA (∇), and silicon substrate (♦) are indicated. (g) SERRS intensities at 1624 and 1397 cm^{-1} of the five Ag nanostructures treated with 10^{-8} M methylene blue.

was further reduced (to ∼30 nm). The corresponding nanostructures were smaller (300 ± 50 nm) than those formed at a ratio of 6, and many clear crevices were observed in the petals (Figure 2d; referred to as Ag-$M_1C_{15}A_{10}$). With 0.1 μmol of MBA and 6 μmol of trisodium citrate (ratio: 60), a few nanoparticles were aggregated, and the corresponding nanostructures (200 ± 30 nm) were composed of several irregularly shaped nanoparticles (Figure 2e; referred to as Ag-$M_{0.1}C_6A_{10}$).

A number of reports on the synthesis of flower-like hierarchical structures using copper,[37] gold,[5,38] silver,[39−42] iron oxide,[43] magnesium oxide,[44] and zinc oxide[45] have been published. These flower-like hierarchical structures were mostly constructed via three growth steps: the generation of small nanoparticles, nanoparticle aggregation, and the subsequent growth of metals/metal oxides from the aggregate surfaces or growth of aggregates with nanoparticles.[5,37,38,43,44] In addition, flower-like Ag nanostructures were also produced by using mandelic and ascorbic acids at low temperatures:[42] the acid molecules formed complexes with Ag^+ ions and/or were adsorbed on Ag nucleates, which subsequently directed the newly formed Ag nanoparticles to assemble into hierarchical nanostructures.

Our hierarchical nanostructures were assumed to be typically synthesized via a mechanism similar to that reported in the literature.[5,37,38,43,44] To further understand the growth mechanism of our nanostructures, the possible roles of the three reducing agents were investigated through additional experiments. First, it appears that MBA directed the hierarchical structure of Ag nanocrystals because, in the absence of MBA, we obtained large and smooth nonhierarchical Ag nanoparticles (Figure S2a, Supporting Information). With an increase in MBA concentration (Figure 2e for 0.1 μmol and Figure S2b, Supporting Information, for 0.5 μmol), the resulting Ag nanostructures displayed a more hierarchical tendency with increased sizes. Furthermore, with 5 μmol of MBA (ratio of trisodium citrate to MBA = 1.2; Figure S2c, Supporting Information), micron-sized and disordered structures were produced. The hierarchical tendency was also indicated by the Ag nanostructures produced with only MBA and ascorbic acid (without the addition of trisodium citrate), as reported elsewhere,[42] and various hierarchical structures were produced. For example, Ag nanosheets were aggregated to form micron-sized particles with 1 μmol of MBA and 10 μmol of ascorbic acid (Figure S3a, Supporting Information); micron-sized flower-like hierarchical Ag nanostructures were produced with increasing MBA concentration (Figure S3b, Supporting Information), and 400 nm nanoclusters resulted from the increase in the concentration of ascorbic acid (Figure S3c, Supporting Information). However, these morphologies deviated from those of the nanostructures shown in Figures 1c and 2b−d and the nanoclusters shown in Figure 2a. Moreover, it was hard to find factors to manipulate the morphologies of hierarchical structures. Therefore, the addition of trisodium citrate might be essential to the morphology-controlled synthesis of flower-like nanostructures. In the presence of Ag nanoclusters, the Ag atoms reduced by ascorbic acid may have been primarily deposited on the nanocluster surfaces to form the hierarchical nanostructures. With an increase in the concentration of ascorbic acid from 10 μmol to 50 and 100 μmol, flower-like Ag nanostructures were still synthesized (Figure S4, Supporting Information). However, the hierarchical structures became more disordered with 100 μmol of ascorbic acid.

We collected TEM images to further investigate the morphologies of the Ag nanostructures shown in Figures 1 and 2 (Figure 3a−e). The petals generated more nanosized gaps from their ends with increasing amounts of trisodium citrate. In addition, a close look at the image revealed that tiny nanoparticles (5−10 nm) were incorporated between the petals (Ag-$M_1C_{1.5}A_{10}$, Figure 3a) or within the gaps (∼20 nm

DOI: 10.1021/acsami.5b03109
ACS Appl. Mater. Interfaces 2015, 7, 14793−14800

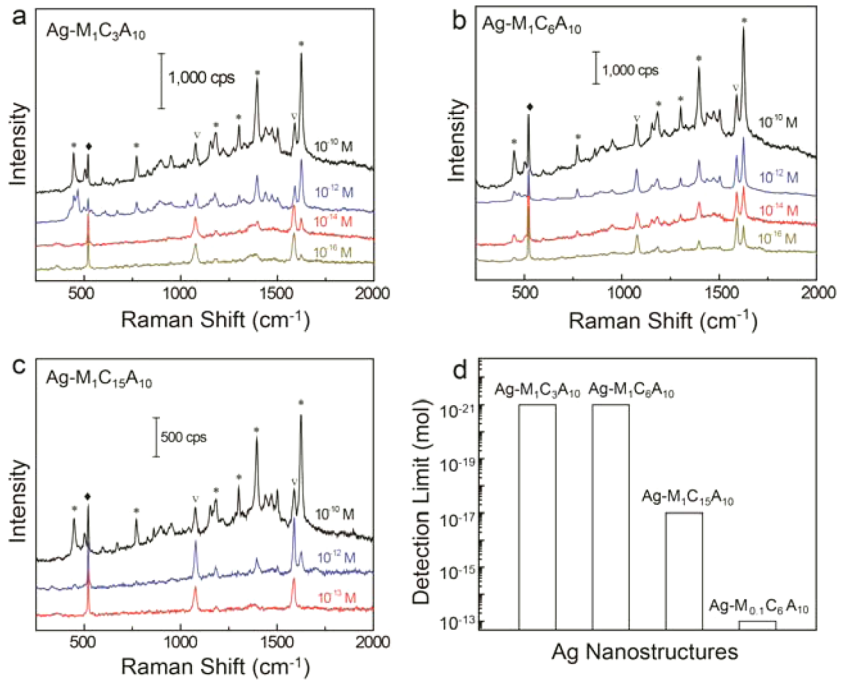

Figure 4. SERRS spectra of the Ag nanostructures for various concentrations of methylene blue: (a) Ag-$M_1C_3A_{10}$, (b) Ag-$M_1C_6A_{10}$, and (c) Ag-$M_1C_{15}A_{10}$. Raman peaks of methylene blue (∗), MBA (∇), and silicon substrate (♦) are indicated. (d) Detection limits of the four Ag nanostructures.

average) generated in the flower petals (Figure 3b–d). These small nanoparticles were likely produced via homogeneous nucleation by ascorbic acid. The number of nanoparticles varied depending on the synthesis conditions; a large number of nanoparticles was observed when Ag-$M_1C_3A_{10}$ or Ag-$M_1C_6A_{10}$ was used. Meanwhile, only irregularly shaped nanostructures were observed when Ag-$M_{0.1}C_6A_{10}$ was used (Figure 3e).

We compared the Raman signal intensities of methylene blue when using the five different types of nanostructures shown in Figure 3a–e as substrates. All the Ag nanostructures were uniformly coated to sufficiently cover the laser beam sizes (1.5 μm) on APTES-modified silicon wafers (see Figures 1d and S5, Supporting Information). Therefore, we could minimize the possible effect of inhomogeneity of surface and/or different concentrations of Ag on the Raman signals. The positively charged amine groups in methylene blue interacted electrostatically with the carboxylic groups on the surfaces of the Ag nanostructures. It is worth noting, through the experiment, that we used a laser having 633 nm, which is very close to the absorption maximum of methylene blue. Due to this reason (resonance effect of methylene blue), the amplification of Raman signals were expected for all the Ag nanostructures we tested:[22−25] thus, it is better to use SERRS, instead of using SERS, for the Raman signals of methylene blue.

First, a 10^{-8} M methylene blue aqueous solution was used to tag the surface of the nanostructures. Generally, as shown in Figure 3f, intense SERRS signals were observed for the nanostructures containing a number of small Ag nanoparticles (Ag-$M_1C_3A_{10}$ and Ag-$M_1C_6A_{10}$) within the nanosized gaps in the Ag petals, whereas the signals were weak or negligible for the nanostructures with smooth petals (Ag-$M_1C_{1.5}A_{10}$), branched petals containing fewer Ag nanoparticles (Ag-$M_1C_{15}A_{10}$), and irregular shapes (Ag-$M_{0.1}C_6A_{10}$; see also Figure S6, Supporting Information). In Figure 3g, we compare the SERS intensities among five nanostructures for the peaks at 1624 cm^{-1} (C−C ring stretching) and 1397 cm^{-1} (C−H in-plane ring deformation).[46−48] The highest SERS intensities were achieved by the nanostructures where many nanoparticles were incorporated within petals (Ag-$M_1C_6A_{10}$); i.e., the values were ∼5 times higher than those with fewer nanoparticles (Ag-$M_1C_{15}A_{10}$) and approximately 150 times higher than those with no small Ag nanoparticles in the petals (Ag-$M_{0.1}C_6A_{10}$).

We further investigated the detection sensitivities of the three Ag nanostructures shown in Figure 3b–d by decreasing the concentration of methylene blue (Figure 4). Interestingly, for the Ag nanostructures shown in Figure 3b (Ag-$M_1C_3A_{10}$) and Figure 3c (Ag-$M_1C_6A_{10}$), significant SERRS signals were detected even at a methylene blue concentration of 10^{-16} M (Figure 4a,b), which essentially corresponds to 10^{-21} mol (because we used 10 μL of 10^{-16} M). Among the plasmonic nanostructures with methylene blue,[49−54] Jana et al.[49] reported 10^{-12} M as a detection limit with Ag plate on alumina support. Sinha et al.[50] reported 10^{-12} M with Au-coated ZnO nanorods with a laser wavelength of 632.8 nm. It is rather cautious to compare our present detection limit with the literature values due to some different experimental conditions, but the present record is the lowest value until now. To minimize the resonance effect of a dye molecule, we further investigated the sensitivity of the Ag-$M_1C_6A_{10}$ with Rhodamine 6G, which weakly absorbs at 633 nm. A significant SERS signal was recorded with 10^{-9} M of this dye (see Figure S7, Supporting Information). For similar plasmonic hierarchical nanostructures,[5,39,42,55] 10^{-4} M with Rhodamine 6G,[39] 5 ppm with melamine,[42] and 10^{-8} M with 4-mercaptobenzoic acid[55] were reported, respectively. Putting this together, the present result is worth demonstrating that our hierarchical Ag nanostructures are having a high potentiality to detect a trace of Raman molecules.

To better understand the morphology-dependent SERRS sensitivity, we next investigated the electric field distribution for

DOI: 10.1021/acsami.5b03109
ACS Appl. Mater. Interfaces 2015, 7, 14793−14800

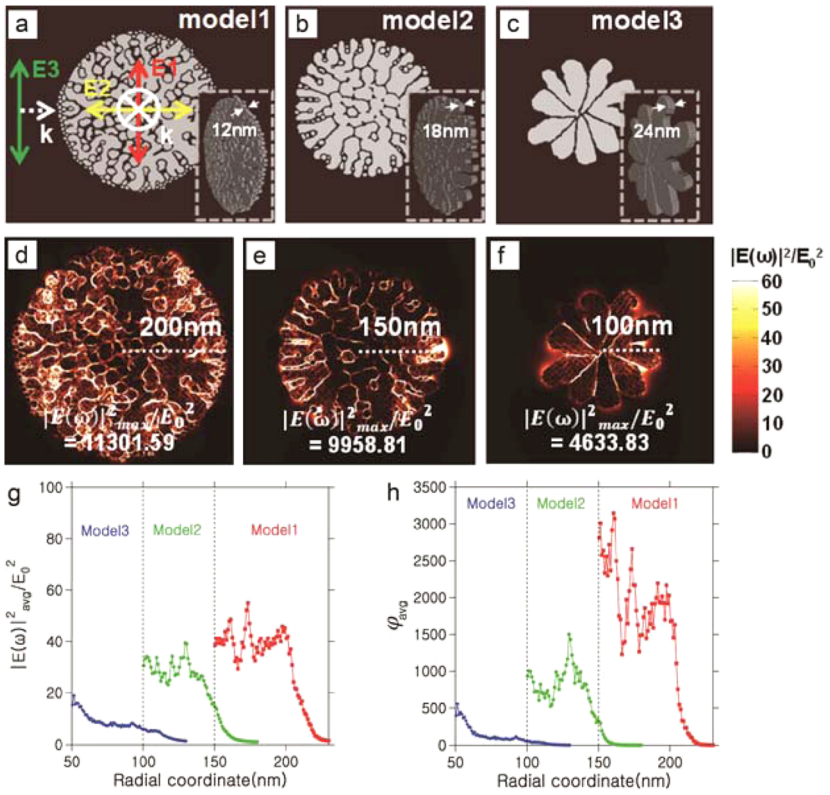

Figure 5. (a–c) Computational models 1, 2, and 3 representing Figure 3d–f, respectively, where *k* is the direction of the incident light and E1, E2, and E3 are the directions of the electric fields. Each model contains the number of dipoles of 247 464, 240 651, and 151 440, respectively, with the dipole space of 2 nm. (d–f) Contour plots of the induced electric fields for models 1, 2, and 3, respectively, based on the E1 direction at an incident wavelength of 633 nm. (g) Average values of $|E(\omega)|^2/E_0^2$ of E1 to E3 directions with a radial coordinate at a wavelength of 633 nm. (h) Average SERS enhancement factor, φ_{avg}, with a radial coordinate.

the three nanostructures (Figures 3c–e) using a computational method by establishing three models (Figure 5): Ag petals generating many nanosized gaps with many nanoparticles between the gaps (model 1 simulating Figures 3c and 5a,c), Ag petals generating nanosized gaps but with fewer nanoparticles (model 2 simulating Figures 3d and 5b,d), and nanostructures with no nanoparticles (model 3 simulating Figures 3e and 5c,e). We used the discrete dipole approximation method. The sizes of models 1 to 3 agree with the average sizes obtained by experimental measurements, and the averaged intensity was calculated over the radial-shell area to exclude the dependence on particle size. Each model contains the number of dipoles of 247 464, 240 651, and 151 440, respectively, with the dipole space of 2 nm. By averaging the induced electric fields in three directions (i.e., E1, E2, E3), the intensity of the induced electric field (i.e., the enhancement factor $|E(\omega)|^2/E_0^2$) in the outer-shell region) was observed to be on the order of the intensities measured for models 1, 2, and 3 (Figure 5g). To evaluate the experimental SERS intensity, the SERS enhancement factor φ, which is a product of enhancement factors at the targeted (i.e., 633 nm) and Stokes-shifted (i.e., 705.53 nm) wavelengths, was obtained and is shown in Figure 5h. The results clearly indicate a large enhancement effect on the electric field, which is primarily attributed to the existence of a number of small Ag nanoparticles in the gaps of the nanostructures. To estimate the collective effect of the petals on the enhancement, we also obtained the extinction spectra (see Figure S8a, Supporting Information), the intensities of which were on the same order as the induced electric field at the incident wavelength of 633 nm; furthermore, we compared the UV–vis extinction spectra from the three synthesized nanostructures (Figure S8b, Supporting Information). The trends of the computational enhancements are in agreement with those observed for the experimental extinction spectra. We note that certain discrepancies exist at high wavelengths, which may have resulted from the use of a limited version of the model systems (i.e., a small portion of the petals).

4. CONCLUSIONS

Ag- and Au-based flower-like nanostructures were previously considered possible SERS substrates with high concentrations of Raman-active molecules.[5,39,42,55] However, a strategy has not yet been reported to enhance/modulate the electric fields of the hierarchical nanostructures to further enhance the corresponding SERS/SERRS signals. In the current study, we developed a synthetic route to engineer the morphologies of flower-like hierarchical Ag nanostructures for use as ultrasensitive SERRS substrates. On the basis of the results of both experimental and theoretical studies, we suggest that the nanostructure composed of flower petals with nanosized gaps and tiny nanoparticles located between the gaps enhances the electric fields. Combining the enhanced field effect with resonance effect of a Raman-active molecule (methylene blue) at a specific wavelength, the Ag nanostructures provided an effective substrate for the detection of methylene blue even if the nanostructures are treated with 10^{-16} M (corresponding to 10^{-21} mol) of tag molecules. Therefore, we suggest that the proposed method provides highly promising nanostructures for SERRS/SERS-based applications.

DOI: 10.1021/acsami.5b03109
ACS Appl. Mater. Interfaces 2015, 7, 14793–14800

■ ASSOCIATED CONTENT

Supporting Information

XRD patterns of the nanostructures, SEM images for various Ag nanostructures obtained during the mechanistic studies, SERRS studies of Ag-$M_{0.1}C_6A_{10}$ by using different concentrations of methylene blue, SERS studies of Ag-$M_1C_6A_{10}$ with Rhodamine 6G, theoretical extinction spectra of the three model Ag nanostructures, and experimental extinction spectra of Ag nanostructures used for the model Ag nanostructures. The Supporting Information is available free of charge on the ACS Publications website at DOI: 10.1021/acsami.5b03109.

■ AUTHOR INFORMATION

Corresponding Authors

*E-mail: skkwak@unist.ac.kr (S.K.K.).
*E-mail: enjoe@hanyang.ac.kr (E.C.C.).
*E-mail: dhkim@ntu.edu.sg (D.-H.K.).

Notes

The authors declare no competing financial interest.

■ ACKNOWLEDGMENTS

A.D., Y.Z., and D.-H.K. acknowledge financial support from Defense Acquisition Program Administration and Agency for Defense Development under the contract UD140080GD and the Academic Research Funding Tier 1 (RG41/14) of Singapore. S.K.K. and T.K.L. acknowledge funds from NRF (2013R1A1A2007491), the Super Computing Center at UNIST (HPC-UNIST), and PLSI at KISTI. E.C.C. acknowledges financial support from NRF (2012R1A1A1004697) and a KETEP (20133030000300) of South Korea.

■ REFERENCES

(1) Wang, Y.; Yan, B.; Chen, L. SERS Tags: Novel Optical Nanoprobes for Bioanalysis. *Chem. Rev.* **2012**, *113*, 1391−1428.
(2) Cao, Y. W. C.; Jin, R. C.; Mirkin, C. A. Nanoparticles with Raman Spectroscopic Fingerprints for DNA and RNA Detection. *Science* **2002**, *297*, 1536−1540.
(3) Freudiger, C. W.; Min, W.; Saar, B. G.; Lu, S.; Holtom, G. R.; He, C.; Tsai, J. C.; Kang, J. X.; Xie, X. S. Label-Free Biomedical Imaging with High Sensitivity by Stimulated Raman Scattering Microscopy. *Science* **2008**, *322*, 1857−1861.
(4) Tang, H.; Meng, G.; Huang, Q.; Zhang, Z.; Huang, Z.; Zhu, C. Arrays of Cone-Shaped ZnO Nanorods Decorated with Ag Nanoparticles as 3D Surface-Enhanced Raman Scattering Substrates for Rapid Detection of Trace Polychlorinated Biphenyls. *Adv. Funct. Mater.* **2012**, *22*, 218−224.
(5) Xie, J.; Zhang, Q.; Lee, J. Y.; Wang, D. I. C. The Synthesis of SERS-Active Gold Nanoflower Tags for in Vivo Applications. *ACS Nano* **2008**, *2*, 2473−2480.
(6) Jin, Y. Engineering Plasmonic Gold Nanostructures and Metamaterials for Biosensing and Nanomedicine. *Adv. Mater.* **2012**, *24*, 5153−5165.
(7) Xu, X.; Kim, K.; Li, H.; Fan, D. L. Ordered Arrays of Raman Nanosensors for Ultrasensitive and Location Predictable Biochemical Detection. *Adv. Mater.* **2012**, *24*, 5457−5463.
(8) Huang, Y.; Dandapat, A.; Kim, D. H. Covalently Capped Seed-Mediated Growth: A Unique Approach toward Hierarchical Growth of Gold Nanocrystals. *Nanoscale* **2014**, *6*, 6478−6481.
(9) Im, H.; Bantz, K. C.; Lindquist, N. C.; Haynes, C. L.; Oh, S. H. Vertically Oriented Sub-10-nm Plasmonic Nanogap Arrays. *Nano Lett.* **2010**, *10*, 2231−2236.
(10) Cho, W. J.; Kim, Y.; Kim, J. K. Ultrahigh-Density Array of Silver Nanoclusters for SERS Substrate with High Sensitivity and Excellent Reproducibility. *ACS Nano* **2012**, *6*, 249−255.
(11) Wang, H.; Levin, C. S.; Halas, N. J. Nanosphere Arrays with Controlled Sub-10nm Gaps as Surface-Enhanced Raman Spectroscopy Substrates. *J. Am. Chem. Soc.* **2005**, *127*, 14992−14993.
(12) Lim, D. K.; Jeon, K. S.; Kim, H. M.; Nam, J. M.; Suh, Y. D. Nanogap-Engineerable Raman-Active Nanodumbbells for Single-Molecule Detection. *Nat. Mater.* **2010**, *9*, 60−67.
(13) Abu Hatab, N. A.; Oran, J. M.; Sepaniak, M. J. Surface-Enhanced Raman Spectroscopy Substrates Created via Electron Beam Lithography and Nanotransfer Printing. *ACS Nano* **2008**, *2*, 377−385.
(14) Camargo, P. H. C.; Rycenga, M.; Au, L.; Xia, Y. Isolating and Probing the Hot Spot Formed between Two Silver Nanocubes. *Angew. Chem., Int. Ed.* **2009**, *48*, 2180−2184.
(15) Li, W.; Camargo, P. H. C.; Lu, X.; Xia, Y. Dimers of Silver Nanospheres: Facile Synthesis and Their Use as Hot Spots for Surface-Enhanced Raman Scattering. *Nano Lett.* **2009**, *9*, 485−490.
(16) Rodríguez-Lorenzo, L.; Álvarez-Puebla, R. A.; Pastoriza-Santos, I.; Mazzucco, S.; Stéphan, O.; Kociak, M.; Liz-Marzán, L. M.; García de Abajo, F. J. Zeptomol Detection Through Controlled Ultrasensitive Surface-Enhanced Raman Scttering. *J. Am. Chem. Soc.* **2009**, *131*, 4616−4618.
(17) Campion, A.; Kambhampati, P. Surface-Enhanced Raman Scattering. *Chem. Soc. Rev.* **1998**, *27*, 241−250.
(18) Alvarez-Puebla, R. A.; Agarwal, A.; Manna, P.; Khanal, B. P.; Aldeanueva-Potel, P.; Carbó-Argibay, E.; Pazos-Pérez, N.; Vigderman, L.; Zubarev, E. R.; Kotov, N. A.; Liz-Marzán, L. M. Gold Nanorods 3D-Supercrystals as Surface Enhanced Raman Scattering Spectroscopy Substrates for the Rapid Detection of Scrambled Prions. *Proc. Natl. Acad. Sci. U. S. A.* **2011**, *108*, 8157−8161.
(19) Cheng, L.; Ma, C.; Yang, G.; You, H.; Fang, J. J. Hierarchical Silver Mesoparticles with Tunable Surface Topographies for Highly Sensitive Surface-Enhanced Raman Spectroscopy. *J. Mater. Chem. A* **2014**, *2*, 4534−4542.
(20) De Angelis, F.; Gentile, F.; Mecarini, F.; Das, G.; Moretti, M.; Candeloro, P.; Coluccio, M. L.; Cojoc, G.; Accardo, A.; Liberale, C.; Zaccaria, R. P.; Perozziello, G.; Tirinato, L.; Toma, A.; Cuda, G.; Cingolani, R.; Di Fabrizio, E. Breaking the Diffusion Limit with Super-Hydrophobic Delivery of Molecules to Plasmonic Nanofocusing SERS Structures. *Nat. Photonics* **2011**, *5*, 682−687.
(21) Lim, D. K.; Jeon, K. S.; Hwang, J. H.; Kim, H.; Kwon, S.; Suh, Y. D.; Nam, J. M. Highly Uniform and Reproducible Surface-Enhanced Raman Scattering from DNA-Tailorable Nanoparticles with 1-nm Interior Gap. *Nat. Nanotechnol.* **2011**, *6*, 452−460.
(22) Lee, P. C.; Meisel, D. Adsorption and Surface-Enhanced Raman of Dyes on Silver and Gold Sols. *J. Phys. Chem.* **1982**, *86*, 3391−3395.
(23) Hildebrandt, P.; Stockburger, M. Surface-Enhanced Resonance Raman Spectroscopy of Rhodamine 6G Adsorbed on Colloidal Silver. *J. Phys. Chem.* **1984**, *88*, 5935−5944.
(24) Graham, D.; Smith, W. E.; Linacre, A. M. T.; Munro, C. H.; Watson, N. D.; White, P. C. Selective Detection of Deoxyribonucleic Acid at Ultralow Concentrations by SERRS. *Anal. Chem.* **1997**, *69*, 4703−4707.
(25) Nicolai, S. H. A.; Rubim, J. C. Surface-Enhanced Resonance Raman (SERR) Spectra of Methylene Blue Adsorbed on a Silver Electrode. *Langmuir* **2003**, *19*, 4291−4294.
(26) Devoe, H. Optical Properties of Molecular Aggregates. I. Classical Model of Electronic Absorption and Refraction. *J. Chem. Phys.* **1964**, *41*, 393−400.
(27) Devoe, H. Optical Properties of Molecular Aggregates. II. Classical Theory of the Refraction, Absorption, and Optical Activity of Solutions and Crystals. *J. Chem. Phys.* **1965**, *43*, 3199−3208.
(28) Turner, M. D.; Hossain, M. M.; Gu, M. The Effects of Retardation on Plasmon Hybridization within Metallic Nanostructures. *New J. Phys.* **2010**, *12*, 083062.
(29) Purcell, E. M. Pennypacker, Scattering and Absorption of Light by Nonspherical Dielectric Grans. *Astrophys. J.* **1973**, *186*, 705−714.
(30) Clausius, R. *Die mechanische Wärmetheorie*; F. Vieweg und Sohn: Braunschweig, 1879; pp 62−97.

DOI: 10.1021/acsami.5b03109
ACS Appl. Mater. Interfaces 2015, 7, 14793−14800

(31) Draine, B. T. The Discrete-Dipole Approximation and Its Application to Interstellar Graphie Grains. *Astrophys. J.* **1988**, *333*, 848−872.
(32) Draine, B. T.; Flatau, P. J. Discrete-Dipole Approximation for Scattering Calculations. *J. Opt. Soc. Am. A* **1994**, *11*, 1491−1499.
(33) Johnson, P. B.; Christy, R. W. Optical Constants of the Noble Metals. *Phys. Rev. B* **1972**, *6*, 4370−4379.
(34) Yang, W. H.; Schatz, G. C.; Vanduyne, R. P. Discrete Dipole Approximation for Calculating Extinction and Raman Intensities for Small Particles with Arbitrary Shapes. *J. Chem. Phys.* **1995**, *103*, 869−875.
(35) Kim, T. Y.; Kim, W. J.; Hong, S. H.; Kim, J. E.; Suh, K. S. Ionic-Liquid-Assisted Formation of Silver Nanowires. *Angew. Chem., Int. Ed.* **2009**, *48*, 3806−3809.
(36) Qi, L.; Lee, B. I.; Chen, S.; Samuels, W. D.; Exarhos, G. J. High-Dielectric-Constant Silver-Epoxy Composites as Embedded Dielectrics. *Adv. Mater.* **2005**, *17*, 1777−1781.
(37) Ge, J.; Lei, J.; Zare, R. N. Protein-Inorganic Hybrid Nanoflowers. *Nat. Nanotechnol.* **2012**, *7*, 428−432.
(38) Fang, J.; Du, S.; Lebedkin, S.; Li, Z.; Kruk, R.; Kappes, M.; Hahn, H. Gold Mesostructures with Tailored Surface Topography and Their Self-Assembly Arrays for Surface-Enhanced Raman Spectroscopy. *Nano Lett.* **2010**, *10*, 5006−5013.
(39) Fang, J.; Yi, Y.; Ding, B.; Song, X. A Route to Increase the Enhancement Factor of Surface Enhanced Raman Scattering (SERS) via a High Density Ag Flower-Like Pattern. *Appl. Phys. Lett.* **2008**, *92*, 131115.
(40) Han, S. H.; Park, L. S.; Lee, J. S. Hierarchically Branched Silver Nanostructures (HBAgNSs) as Surface Plasmon Regulating Platform for Multiplexed Colorimetric DNA Detection. *J. Mater. Chem.* **2012**, *22*, 20223−20231.
(41) Liang, H.; Li, Z.; Wang, W.; Wu, Y.; Xu, H. Highly Surface-Roughened "Flower-Like" Silver Nanoparticles for Extremely Sensitive Substrates of Surface-Enhanced Raman Scattering. *Adv. Mater.* **2009**, *21*, 4614−4618.
(42) Zhang, B.; Xu, P.; Xie, X.; Wei, H.; Li, Z.; Mack, N. H.; Han, X.; Xu, H.; Wang, H. L. Acid-Directed Synthesis of SERS-Active Hierarchical Assemblies of Silver Nanostructures. *J. Mater. Chem.* **2011**, *21*, 2495−2501.
(43) Zhong, L. S.; Hu, J. S.; Liang, H. P.; Cao, A. M.; Song, W. G.; Wan, L. J. Self-Assembled 3D Flowerlike Iron Oxide Nanostructures and Their Application in Water Treatment. *Adv. Mater.* **2006**, *18*, 2426−2431.
(44) Fang, X. S.; Ye, C. H.; Zhang, L. D.; Zhang, J. X.; Zhao, J. W.; Yan, P. Direct Observation of the Growth Process of MgO Nanoflowers by a Simple Chemical Route. *Small* **2005**, *1*, 422−428.
(45) Ahmad, M.; Yingying, S.; Nisar, A.; Sun, H.; Shen, W.; Wei, M.; Zhu, J. Synthesis of Hierarchical Flower-Like ZnO Nanostructures and Their Functionalization by Au Nanoparticles for Improved Photocatalytic and High Performance Li-Ion Battery Anodes. *J. Mater. Chem.* **2011**, *21*, 7723−7729.
(46) D'Andrea, C.; Bochterle, J.; Toma, A.; Huck, C.; Neubrech, F.; Messina, E.; Fazio, B.; Maragò, O. M.; Di Fabrizio, E.; de La Chapelle, M. L.; Gucciardi, P. G.; Pucci, A. Optical Nanoantennas for Multiband Surface-Enhanced Infrared and Raman Spectroscopy. *ACS Nano* **2013**, *7*, 3522−3531.
(47) Gehan, H.; Fillaud, L.; Chehimi, M. M.; Aubard, J.; Hohenau, A.; Felidj, N.; Mangeney, C. Thermo-Induced Electromagnetic Coupling in Gold/Polymer Hybrid Plasmonic Structures Probed by Surface-Enhanced Raman Scattering. *ACS Nano* **2010**, *4*, 6491−6500.
(48) Xiao, G. N.; Man, S. Q. Surface-Enhanced Raman Scattering of Methylene Blue Adsorbed on Cap-Shaped Silver Nanoparticles. *Chem. Phys. Lett.* **2007**, *447*, 305−309.
(49) Jana, D.; Mandal, A.; De, G. High Raman Enhancing Shape-Tunable Ag Nanoplates in Alumina: A Reliable and Efficient SERS Technique. *ACS Appl. Mater. Interfaces* **2012**, *4*, 3330−3334.
(50) Sinha, G.; Depero, L. E.; Alessandri, I. Recyclable SERS Substrates Based on Au-Coated ZnO Nanorods. *ACS Appl. Mater. Interfaces* **2011**, *3*, 2557−2563.
(51) Lee, H. K.; Lee, Y. H.; Phang, I. Y.; Wei, J.; Miao, Y. E.; Liu, T.; Ling, X. Y. Plasmonic Liquid Marbles: A Miniature Substrate-less SERS Platform for Quantitative and Multiplex Ultratrace Molecular Detection. *Angew. Chem., Int. Ed.* **2014**, *53*, 5054−5058.
(52) Panikkanvalappil, S. R.; El-Sayed, M. A. Gold-Nanoparticle-Decorated Hybrid Mesoflowers: An Efficient Surface-Enhanced Raman Scattering Substrate for Ultra-trace Detection of Prostate Specific Antigen. *J. Phys. Chem. B* **2014**, *118*, 14085−14091.
(53) Fales, A. M.; Yuan, H.; Vo-Dinh, T. Silica-Coated Gold Nanostars for Combined Surface-Enhanced Raman Scattering (SERS) Detection and Singlet-Oxygen Generation: A Potential Nanoplatform for Theranostics. *Langmuir* **2011**, *27*, 12186−12190.
(54) Lu, G.; Li, H.; Liusman, C.; Yin, Z.; Wu, S.; Zhang, H. Surface Enhanced Raman Scattering of Ag or Au Nanoparticle-Decorated Reduced Graphene Oxide for Detection of Aromatic Molecules. *Chem. Sci.* **2011**, *2*, 1817−1821.
(55) He, J.; Han, J.; Yan, J.; Kang, L.; Zhang, B.; Du, Y.; Dong, C.; Wang, H.-L.; Xu, P. Fast Fabrication of Homogeneous Silver Nanostructures on Hydrazine Treated Polyaniline Films for SERS Applications. *CrystEngComm* **2012**, *14*, 4952−4954.

DOI: 10.1021/acsami.5b03109
ACS Appl. Mater. Interfaces 2015, 7, 14793−14800